Chapter 8
Mammography Phantoms

Alessandra Tomal

8.1 Introduction

Mammography is considered the preferred technique for early detection of the breast cancer. Due the similarity on the elemental composition of the normal and abnormal tissues that comprise the breast, and also due the small size of the breast nodules in the early stage, the optimization of IQ and dose in mammography is a critical factor [69].

Breast phantoms play an important role in the optimization process in mammography through the assessment of IQ and accurate determination of dose, quality control (QC), and quality assurance (QA) in mammography; optimization of specific imaging tasks, such as detection of masses and microcalcifications, dosimetry in mammography, and characterization of the performance of an imaging system [1, 22, 41, 56, 69]. Breast phantoms have also been used for comparison of the performance of different equipment and technologies. In addition, optimization of exposure techniques and study of new imaging technologies, such as dual-energy mammography, contrast-enhanced dual-energy mammography, digital breast tomosynthesis, and breast CT [5, 7, 49, 57, 58] involve a large application of mammographic phantoms.

The main requirement for a breast phantom is the composition with tissue-equivalent material, which reproduces the attenuation properties of the human breast tissues. The material needs to be stable over time and can be moldable [56, 68]. The most used tissue-equivalent materials are plastic (i.e., PMMA—polymethyl methacrylate) or epoxy resins [68], which represents breasts composed of different percentages of adipose and glandular tissues, based on breast composition presented in the literature [33, 40, 70]. Although the breast tissue-equivalent material can be manufactured using components which have similar composition and densities to

A. Tomal (✉)
Institute of Physics, Federal University of Goiás, Campus Samambaia, Caixa Postal 131Goiânia, Goiás 74001-970, Brazil
e-mail: alessandra_tomal@yahoo.com.br; atomal@if.ufg.br

L. A. DeWerd and M. Kissick (eds.), *The Phantoms of Medical and Health Physics*, Biological and Medical Physics, Biomedical Engineering,
DOI: 10.1007/978-1-4614-8304-5_8,

the real breast tissues, studies point to the need for a careful analysis to choose the most adequate material to simulate the scattering properties of different breast compositions [42, 56].

The breast phantoms are also designed to be realistically shaped and molded to represents the real breast dimensions in simple uniform blocks or highly detailed design, containing embedded inserts that mimic clinically relevant features of the normal and pathological structures and background within the breast.

Since 1980s, the screen–film mammography was considered the gold technique for early detection of breast cancer. In this technique, the use of breast phantoms was essential for establishment of QC and QA programs for monitoring both IQ and radiation dose in the mammographic examination [1, 25, 38, 39]. Recently, digital mammography is gradually replacing the conventional film–screen mammography in most countries [26, 39, 49]. Consequently, it is in progress an important activity related to the development of QC protocols [39] and optimization of this digital technology [7, 18, 58, 67]. Moreover, novel breast imaging techniques, such as dual-energy mammography, contrast-enhanced dual-energy mammography, digital breast tomosynthesis, and breast CT, have justified the necessity for developing new breast phantoms containing specific features to be used for IQ and dose assessment of these contemporary technologies [12, 13, 57].

8.2 Phantoms for Imaging

8.2.1 Phantom for Quality Control and Accreditation Programs

High IQ is fundamental in mammographic screening programs, in order to improve the sensitivity of the exam for the early detection of breast pathologies. In this context, breast phantoms play a fundamental role to establish, assess, and optimize IQ in mammography. Breast phantoms are also used for accreditation of new mammography facilities for both screen–film and full-field digital mammography (FFDM) systems.

Breast test phantoms to evaluate IQ could contain embedded inserts that mimic the anatomical breast structures and/or artificial features such as low-contrast details, microcalcifications, fibers, high-contrast frequency patterns, and step wedges, which are used to evaluate high- and low-contrast object detection, spatial resolution, noise response, and detectability threshold [12, 22, 41, 44, 69].

In general, test phantom assessment criteria in accreditation programs for screening mammography are subjective [35], being based on IQ scores defined from detail visibility of different targets, such as microcalcifications and low-contrast masses and fibers [1, 14, 25]. The basic condition of the utilization of an IQ phantom is that a given dimension of group structures should be visualized in a

mammographic image, even if the phantom is imaged on different machines applying different procedures.

The main test phantoms available for the purpose of IQ assessment in mammography are described below. One of the first phantoms developed to contain insert structures mimicking those found in a clinical mammography was the Bart test phantom, which was described in 1980 by White and Tucker [69]. The Bart test phantom was originally designed to be used for assessing IQ in mammography and for comparison purposes of UK breast imaging practice by the Hospital Physicists' Association [29]. The phantom was formulated to be composed of epoxy resin BR12 [68], simulating the composition of an average breast tissue, representing a homogeneous mixture of 50 % adipose tissue and 50 % water. Inside the BR12 phantom, test inserts were included to evaluate different structures and materials on the IQ, being basically the following: adipose and water-like structures, calcifications, and skin step edge. The structures of interest present inside the phantom had different geometric shapes and dimension, and they were composed of epoxy resin-based substitutes, aluminum oxide, and silicon. The Bart phantom was designed to evaluate the performance of IQ in mammography combined in different ways, allowing assess to the contrast and resolution of mammographic devices. However, the use of this phantom for practical evaluation of several mammographic devices shows some difficulties, since it was never available commercially and it is also little sensitive to changes in tube potential and focal spot size [45].

Due to the importance of evaluating IQ in mammography using test objects, many efforts were done to develop a breast phantom that has greater sensitivity to changes in tube potential and better discrimination between different equipment and image receptor. In this context, several phantoms were produced and are described below.

In 1987, the test phantom Leeds TOR[MAX] was developed to implement routine QC procedures within the U.K. National Breast Cancer Screening Programme [16, 17]. TOR[MAX] comprises D-shaped PMMA plates, representing the average 50 % adipose–50 % glandular (50:50) breast. An additional TOR [MAX] test object includes different types of structures in a homogeneous background: high- and low-contrast bar patterns, low-contrast discs, and a step wedge [21, 28]. The test pattern and details included on the Leeds TOR[MAX] phantom provide quantitative information for IQ purposes, allowing the measurement of grayscale rendition, high-contrast spatial resolution, and both large- and small-area detail detectability [16]. In 1992, it was developed a supplementary test phantom TOR[MAM], which contains details that provides a radiological image with an appearance more closely to that achieved during a clinical mammographic examination [16]. TOR[MAM] phantom also comprises a D-shaped PMMA test object divided in two halves, which include different types of test details. One half of this phantom is designed for quantitative evaluation and contains groups of fibers, calcifications, and low-contrast discs composed of equivalent breast-tissue materials. The other half contains structures that mimic breast tissue with groups of microcalcifications, simulating a clinical mammographic image [74]. Such phantoms have been used in several studies

concerning the IQ performance of imaging system for screen–film, computed radiography, FFDM, and image processing of digital imaging [16, 21]. With the advent of novel 3D breast imaging techniques, as digital breast tomosynthesis, the use of such test phantom is also showed to be useful for evaluation of digital breast image reconstruction algorithms [9].

Kimme-Smith et al. [41] compared several mammography test objects (commercially available and prototype) with respect to their resolution and contrast targets and the dose. In this study, the authors observed a great variation on the quantities evaluated with the phantom and details compositions and also described the need for a reliable phantom for evaluating the IQ and dose in mammography.

Law [44] described the construction of the Du Pont mammographic test phantom, constituted by a PMMA block with 12 × 12 cm area and total thickness of 4 cm, simulating an average 50:50 breast. The phantom was developed to contain high-contrast bar patterns and different structures that mimic clinical mammographic features, such as microcalcifications, fibrous structures, and small spherical objects, which allow the assessment of minimum detail contrast and resolution score. The developed phantom has been found to have better sensitivity and discrimination, making it suitable for studying the IQ performance in mammography.

In the last decades, several national and international protocols for mammography QC program have pointed to the importance of using a mammographic accreditation phantom to perform the image QC of mammographic systems in the QC and QA programs [1, 25, 38, 39]. The American College of Radiology (ACR) introduced a standard accreditation phantom (ACR phantom) [6, 22, 34, 48] to access the image for QC purposes in the mammography accreditation program (MQA). The ACR phantom simulates a 50:50 breast of 4.5 cm thickness, and it consists of a PMMA block and a wax block containing the test structures of known size, shape, and density (Fig. 8.1). The structures included in the wax insert consist of nylon fibrils, groups of microcalcifications, and lens-shaped masses, representing different structures or malignancies similar to those found clinically when imaging a real breast. The visibility of these structures in the radiographic image ranges from visible to invisible, defining a visibility threshold and giving a global IQ score [24, 37, 48]. Performance of this imaging quality test is an important factor in the accreditation of a facility [14].

The ACR phantom has been used for assessing IQ in both film–screen mammography and FFDM; however, phantoms designed for screen/film mammography could show low sensitivity in FFDM [36, 37, 47, 62]. Huda et al. [37] showed that the ACR phantom is unsatisfactory for assessing IQ in FFDM and it requires modifications to have the appropriate range and sensitivity for current digital mammography imaging systems available [32]. Besides, there are several commercially available digital mammography accreditation phantoms (Gammex, Radiation Measurements Inc.; CIRS—Computerized Imaging Reference Systems Inc). The composition of the phantom and the included structures are the same as in the ACR phantom; however, the phantom thickness and the number of inserted objects are different, and they have smaller sizes. In addition, Song et al. [62]

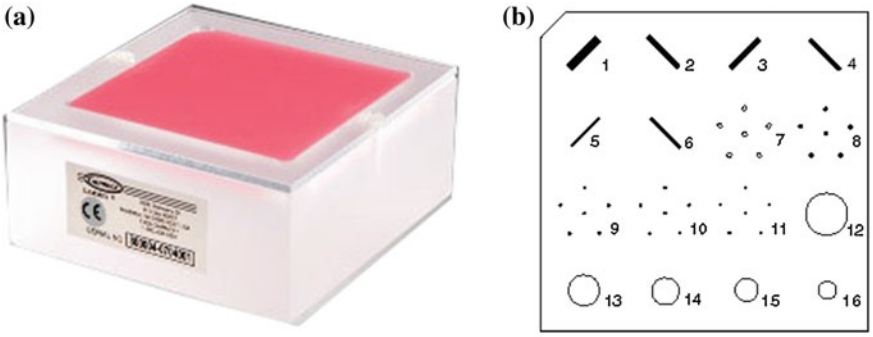

Fig. 8.1 **a** ACR phantom and **b** structures layout (Model 156, Gammex—RMI Radiation Measurements Inc., Middleton, WI) http://www.gammex.com/ace-files/Gammex_Catalog.pdf

compared the ACR phantom and digital mammography accreditation phantom in terms of the signal-to-noise ratio (SNR) and the visibility of the inserted objects for assessment of IQ on FFDM. The authors concluded that ACR accreditation phantom is superior, being satisfactory for assessing the IQ in FFDM, if appropriate voltage and current–time product settings are kept during phantom image acquisition.

Recently, many countries have developed their own mammography QC program, regulating the minimum IQ performance and doses related to a mammographic examination. In Brazil, for example, the Brazilian College of Radiology (CBR) and the National Agency for Health Surveillance (ANVISA) recommend standards of practice for mammography, in which the IQ assessment should be performed using a specific test object (CDM-phantom MAMA) developed for this purpose. The commercially available CDM-phantom MAMA was developed in Brazil, and it presents similarities to the ACR phantom, being composed of PMMA plates and a wax insert region, containing different detail objects: high-contrast bar pattern, microcalcifications, fibers, tumor-like masses, and low-contrast details. This phantom is widely used for mammographic QC in different facilities in Brazil and also for studies on IQ and dosimetry [53].

In addition to the standard plastic breast phantom, as the PPMA, other breast phantoms with different composition were proposed to evaluate the performance of mammographic systems in terms of IQ, based on the composition of breast tissues and breast geometry described by Hammerstein et al. [33]. The commercially available CIRS phantom models 010 and 011A (CIRS, Inc., Norfolk, VA) for IQ assessment are made of D-shaped epoxy resin-equivalent material, simulating breast of different thickness, and glandular content within an external shield layer of simulating adipose tissue. This phantom allows a detailed evaluation of a mammographic system for several normal and pathological breast structures, consisting of microcalcifications, high-contrast resolution pattern, low-contrast masses, line-pair test pattern, and a step wedge.

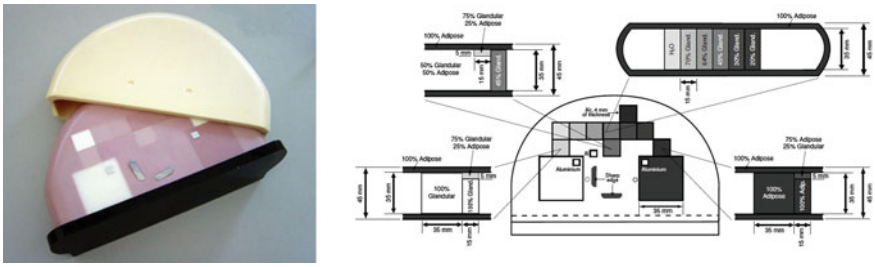

Fig. 8.2 Test phantom developed by Pachoud et al. [54]

In 2004, a new test phantom was also developed for IQ evaluation in digital and conventional mammography by Pachoud et al. [54]. The authors developed a prototype test phantom, composed of CIRS equivalent materials. A 35-mm layer of 50:50 glandular/adipose tissue equivalent is surrounded by a 5-mm-thick covering of 100 % adipose equivalent material, representing the breast model proposed by Hammerstein et al. [33]. The phantom comprises regions with different tissue compositions (100 % adipose, 50:50 mixture, and 100 % glandular) and includes structures which are used to evaluate several IQ features, such as low- and high-contrast resolution, spatial resolution, and image noise (Fig. 8.2). A step wedge with different glandular/adipose compositions is included within the central layer for signal output calibration. The test phantom also contains two areas composed of 100 % glandular- and 100 % adipose-equivalent breast tissue, which can be used for assessment of noise power spectra. Two holes are included on the phantom's top surface, at 60 mm from the chest wall, which can hold thermoluminescent dosimeters (TLD) for entrance skin dose measurements. The new test phantom proposed by Pachoud et al. [54] proved to be useful for assessments of several IQ parameters (contrast, dynamic range, spatial resolution, and noise) for conventional and digital mammography equipments, allowing to compare different image systems. Otherwise, this phantom should be used as complement to another phantom in assessment of IQ in mammography, since it does not contain structures for detections tasks.

8.2.2 Contrast–Detail Phantom

The success of a mammographic screening program is related with the production of high-quality images, which provides the maximum diagnostic information in order to distinguish tissue alterations within the breast with very low contrast and small size. Contrast–detail (CD) detection measurement is the technique most used for assessing the performance of an imaging system based on identification of small alterations [15, 66]. In the CD experiment, the observers record the small size of object that they perceive, at a given confidence level, on the image of

simple objects that vary both in diameter and contrast. Thompson and Faulkner [66] described a CD test phantom for screen–film mammography, containing series of discs of varying attenuation and diameter, which were chosen to simulate significant structures in a mammographic image, such as low-contrast tissue masses and higher-contrast small object such as microcalcifications.

The importance of CD measurements for assess the IQ performance of mammographic devices has been recognized, and this test has been included in several protocols. The European guidelines [26] for the QC in digital mammography define threshold contrast standards for digital mammography, based on CD measurements, in order to ensure that digital mammography systems have a performance at least as well as film–screen systems. This test is usually performed by using the commercially available Nijmegen CDMAM (Artinis Medical Systems) CD phantom, which consists of an aluminum base with gold discs of various thickness and diameter, attached to PMMA cover block (Fig. 8.3) [8].

The use of CD test phantom in screen–film and digital mammography has demonstrated a large potential in several applications. Robson et al. [59] used a CD phantom to establish optimal optical density values for two mammographic film–screen combinations, based on the signal-to-noise ratio (SNR). Berns et al. [7] have employed a CD test phantom to determine the optimal exposure technique in FFDM compared to screen–film mammography, including the comparison of the performance of different analog and digital mammography systems. With the advent of digital mammography systems, the CD test phantom plays a fundamental role for evaluating the effect of pixel size on the detection of simulated microcalcifications in digital mammography, as described by Suryanarayanan et al. [63], who used the CDMAM phantom.

Novel mammographic IQ test phantom design has been proposed as a cheaper alternative for image QA and evaluation of the CD score for the breast screening programs [43, 65]. The phantom developed by Kotre and Porter [43] was based on LaserJet printed test features on a Mylar projector transparency, on which the test features are composed of 50 % by weight of iron oxide present in the toner. The low-contrast test features are sandwiched between two PMMA blocks. Despite the

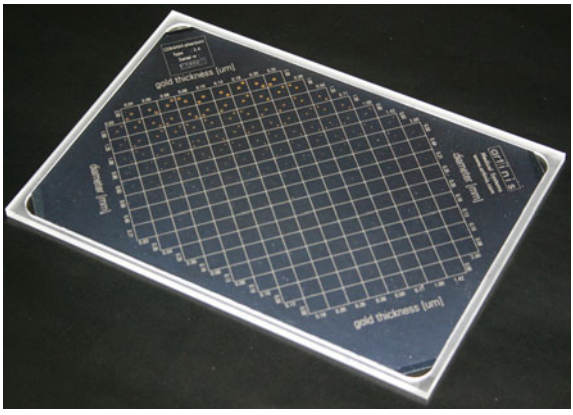

Fig. 8.3 Nijmegen CDMAM contrast–detail phantom (http://www.artinis.com/product/cdmam_34)

simplified manufacture process, this novel test phantom design is cheaper, more flexible, and offers a performance similar to other commercial mammographic CD phantoms in terms of image of low-contrast structures, being a good alternative way for producing test phantoms [43]. However, this phantom has disadvantages, since high-contrast resolution structures cannot be produced through the standard printing process.

8.3 Phantoms for Dosimetry

The knowledge of the absorbed dose to the breast during a mammographic examination is an important topic for QA programs, since it is related to carcinogenesis risk and allows comparisons between different imaging techniques and equipments. In this way, the assessment of the breast dose in a mammographic examination is essential in breast screening programs in which predominantly asymptomatic women are examined.

The mean glandular dose (MGD) is considered the most appropriate quantity for risk assessments associated with mammography, since the glandular tissue is the most vulnerable tissue in the breast [19, 71]. Therefore, the MGD has been recommended by several national and international protocols as the dosimetric parameter to be evaluated in mammography [1, 25, 38, 49].

A direct measurement of MGD is impossible for any individual breast, and in most practical situation, it is derived from the product of the measured entrance air kerma and appropriated conversion factors [49]. The conversion factors were initially measured using an appropriated test phantom [33] and also calculated using Monte Carlo simulation [10, 19, 71].

Breast phantoms are usually employed to estimate the MGD based on measurements of the entrance surface air kerma and half-value layer (HVL) [20, 23]. The entrance air kerma and HVL can be directly measured by placing the ionization chamber at the tube side of the phantom and level with its top surface, positioned to a distance between 4 and 6 cm from the chest wall, defined according the used protocol [1, 25, 50, 51]. The incident air kerma can also be measured using TLD dosimeters placed on the entrance surface of the phantom or breast [1, 25].

The standard breast phantom for dosimetry in mammography usually represents a typical breast composed of a 50:50 mixture of adipose and glandular tissues [20, 33]. Several national and international protocols recommended that the standardized phantom chosen for dose evaluation in mammography is constructed from PMMA, and its thickness ranges from 4 to 5 cm [20, 60, 61].

Although a PMMA standard phantom is widely used for dose measurements, it is a limited approach since it provides a quantitative dose evaluation for only a particular breast tissue composition and thickness. In practice, there is a significant variation in the average breast thickness and composition for a group of women in a given geographical region [20, 72], so that the MGD measured using phantoms is not representative of true breast doses [3]. In this way, the use of phantoms of

different thickness and composition is useful for estimating the MGD for realistic woman population.

Several phantoms have been developed to mimic the radiological properties of different breast tissue, allowing a detailed dose assessment in mammography [31, 68]. The most common phantom is BR12, commercially available originally from Nuclear Associates (Cleveland, OH), today Fluke Biomedical Corporation. This phantom is composed of resin epoxy tissue-equivalent, simulating a tissue composition of 50 % glandular tissue and 50 % adipose tissue and developed by White [68]. CIRS (Norfolk, VA) manufacturer also offers phantom materials of different thicknesses and compositions, simulating 100 % glandular breast to 100 % adipose breasts. These phantoms have been recommended by national and international protocols and have been employed in several countries for studying the MGD with QC purposes [1, 60].

In the last years, new phantoms were developed to provide a more accurate evaluation of MGD. Argo et al. [3] described the construction of breast tissue-equivalent series (BRTES) of phantoms composed of epoxy resin, simulating glandularities from 0 to 100 %. The authors observed that, in comparison with the BRTES phantom, the standard 4-cm-thickness ACR phantom and BR12 are likely to underestimate the MGD for most patients, being the variation dependent on local patient demographics. Almeida et al. [2] produced breast phantoms BTE, based on BRTES tissue-equivalent material, to simulate glandular and adipose tissues, in order to evaluate MGD in mammography. In their work, the authors concluded that BTE phantoms should be used instead of PMMA-based phantoms for appropriate estimate of MGD in mammography, since most of the women present breast grandularity lower than 50 % [31, Young et al. 75, 72].

8.4 Anthropomorphic Phantoms for Mammographic Imaging

Anthropomorphic phantoms were introduced in mammography to provide a more realistic task to the observer, since they mimic the composition and geometric structures of the breast, providing X-ray images similar to those present in a real breast [57]. The first anthropomorphic breast phantom introduced for IQ and dose assessment in mammography was constructed by embedding fixed tissues in plastic [27]. However, these types of phantoms change their characteristics with time, and they cannot be easily reproduced in identical copies. A new concept of anthropomorphic breast phantom was introduced by Caldwell and Yaffe [11] and Yaffe et al. [73], who have developed the “Rachel” phantom. This phantom consists of a breast tissue-equivalent base, simulating the tissue structures, combined with a mercury-enhanced mammogram, which simulates the fine details. The Rachel phantom is commercially available (Gammex RMI, Model 169, Gammex Inc., Middleton, WI), being widely used for mammography quality IQ

and dose studies [46], since it provides realistic breast images simulating the breast architecture and anatomical noise. However, the application of the Rachel phantom is limited to evaluation of 2D projection imaging systems, since this phantom does not mimic the real 3D breast anatomy [11, 12].

On other hand, several anthropomorphic phantoms are constructed by combining tissue-equivalent material spheres of different dimensions and compositions, embedded in a homogeneous background and contained inside a plastic box [4, 55, 64]. Although the image pattern achieved with these phantoms is not similar to a real breast image, the sphere phantom is very simple to construct and can easily produce different background realizations [30]. Sphere phantoms have been widely used for evaluating the IQ and doses in mammography, and also for optimizing the examination procedures of new mammographic techniques, such as dual-energy mammography, contrast-enhanced dual-energy mammography, and digital breast tomosynthesis [4, 55, 64].

The patient dose reduction in FFDM compared with conventional screen–film system has also been studied by analyzing the effect on the detectability of microcalcifications in an anthropomorphic breast phantom, as described by Obenauer et al. [52].

In the last years, CIRS slab phantom (model 020) became commercially available. This phantom is constructed with D-shaped slabs composed of a heterogeneous mixture of two breast-equivalent materials, allowing to create a large number of different backgrounds.

More recently, 3D anthropomorphic phantoms for IQ assessment of 2D and 3D breast X-ray imaging systems have been developed by Carton and coworkers [12,13], based on a computer model that generates breast voxel phantoms (Fig. 8.4). These phantoms are composed of tissue-equivalent materials of varying size, shape, glandularity, and internal composition [12, 13], and they show potential to be used for both qualitative and quantitative performance assessments for 2D and 3D breast X-ray imaging systems. Finally, Freed et al. [30] described an anthropomorphic phantom to be used for both X-ray and MRI breast imaging

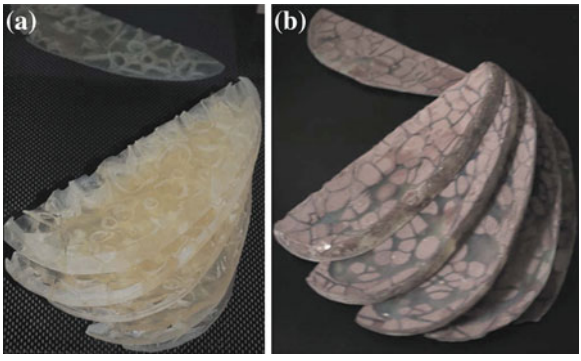

Fig. 8.4 Anthropomorphical phantom developed by Carton et al. [12] **a** Phantom sections of the fibroglandular tissue, skin, and Cooper's ligaments composed by tissue equivalent materia with 50% glandular equivalence **b** Phantom sections after filling the structures with epoxy resin with 100% adipose equivalence

modalities, composed of a mixture of lard and egg white. This phantom proved to be a useful tool for quantitative assessment of IQ in 2D and 3D mammographic techniques, for the purpose of detection and characterization.

8.5 Standard Phantom Use in the Future

The standard breast phantoms used nowadays in QC and QA programs for optimization and accreditation of mammographic equipments represent an average 50 % adipose–50 % glandular breast. However, Geise and Palchevsky [31] and Young et al. 75 have showed that effective glandular content that simulated in the average woman is 35 %. Besides, recently, Yaffe et al. [72] showed that approximately 95 % of the women presented breast glandular content <45 %, while the standard average breast composition is 20 % glandular. In this way, more realistic phantoms should be developed for accurate assessment of IQ and dose in mammography, considering the new standard breast composition.

The introduction of novel 3D X-ray breast imaging techniques, such as digital breast tomosynthesis and breast computed tomography (breast CT), also have significantly increased the need for 3D anthropomorphic breast phantom to properly simulate the breast anatomy [57]. A proper 3D anthropomorphic breast phantom would allow for the evaluation of IQ parameters, thereby optimizing new imaging techniques and reconstruction algorithms for 3D imaging techniques, and also allowing for comparisons to the performance of 2D and 3D imaging techniques [12].

References

1. ACR. (1999). *Mammography quality control manual*. Reston: American College of Radiology.
2. Almeida, C. D., Coutinho, C. M. C., Dantas, B. M., Peixoto, J. E., & Koch, H. A. (2012). A new mammography dosimetric phantom. *Radiation Protection Dosimetry, 151*, 196–198.
3. Argo, W. P., Hintenlang, K., & Hintenlang, A. D. E. (2004). A tissue-equivalent phantom series for mammography dosimetry. *Journal of Applied Clinical Medical Physics, 5*, 112–119.
4. Baldelli, P., Bravin, A., Di Maggio, C., Gennaro, G., Sarnelli, A., Taibi, A., et al. (2006). Evaluation of the minimum iodine concentration for contrast-enhanced subtraction mammography. *Physics in Medicine and Biology, 51*, 4233–4251.
5. Baldelli, P., Phelan, N., & Egan, G. (2010). Investigation of the effect of anode/filter materials on the dose and image quality of a digital mammography system based on an amorphous selenium flat panel detector. *British Journal of Radiology, 83*, 290–295.
6. Barnes, G. T., & Hendrick, R. E. (1994). Mammography accreditation and equipment performance. *Radiographics, 14*, 129–138.
7. Berns, E. A., Hendrick, R. E., & Cutter, G. R. (2003). Optimization of technique factors for a silicon diode array full-field digital mammography system and comparison to screen-film mammography with matched average glandular dose. *Medical Physics, 30*, 334–340.

8. Bijkerk, K. R., Lindeijer, J. M., & Thijssen, M. A. O. P. (1993). The CDMAM phantom: A contrast-detail phantom specifically for mammography. *Radiology, 185*, 395–399.
9. Bliznakova, K., Kolitsi, Z., Speller, R. D., Horrocks, J. A., Tromba, G., & Pallikarakis, N. (2010). Evaluation of digital breast tomosynthesis reconstruction algorithms using synchrotron radiation in standard geometry. *Medical Physics, 37*, 1893–1903.
10. Boone, J. M. (1999). Glandular breast dose for monoenergetic and high-energy x-ray beams: Monte Carlo assessment. *Radiology, 213*, 23–37.
11. Caldwell, C. B., & Yaffe, M. J. (1990). Development of an anthropomorphic breast phantom. *Medical Physics, 17*, 273–280.
12. Carton, A. K., Bakic, P., Ullberg, C., Derand, H., & Maidment, A. D. A. (2011). Development of a physical 3D anthropomorphic breast phantom. *Medical Physics, 38*, 891–896.
13. Carton, A. K., Gavenonis, S. C., Currivan, J. A., Conant, E. F., Schnall, M. D., & Maidment, A. D. A. (2010). Dual-energy contrast-enhanced digital breast tomosynthesis—a feasibility study. *British Journal of Radiology, 83*, 344–350.
14. Chakraborty, D. P., & Eckert, M. P. (1995). Quantitative versus subjective evaluation of mammography accreditation phantom images. *Medical Physics, 22*, 133–143.
15. Cohen, G., McDaniel, D. L., & Wagner, L. K. (1984). Analysis of variations in contrast-detail experiments. *Medical Physics, 11*, 469–473.
16. Cowen, A. R., Brettle, D. S., Coleman, N. J., & Parkin, G. J. S. (1992). A preliminary investigation of the imaging performance of photostimulable phosphor computed radiography using a new design of mammographic quality-control test object. *British Journal of Radiology, 65*, 528–535.
17. Cowen, A. R., & Coleman, N. J. (1991). Physics in diagnostic radiology. Design of test objects and phantoms for quality control in mammographic screening. York, UK, IPEM. IPSM Report 61.
18. Cunha, D. M., Tomal, A., & Poletti, M. E. (2012). Optimization of x-ray spectra in digital mammography through Monte Carlo simulations. *Physics in Medicine and Biology, 57*, 1919–1935.
19. Dance, D. R. (1990). Monte Carlo calculation of conversion factors for the estimation of mean glandular breast dose. *Physics in Medicine and Biology, 35*, 1211–1219.
20. Dance, D. R., Skinner, C. L., & Carlsson, G. A. (1999). Breast dosimetry. *Applied Radiation and Isotopes, 50*, 185–203.
21. Darambara, D. G., Taibi, A., & Speller, R. D. (2002). Image-quality performance of an a-Si: H-based X-ray imaging system for digital mammography. *Nuclear Instruments and Methods in Physical Research Section A, 477*, 521–526.
22. DeWerd, L. A., Wochos, J., & Cameron, J. (1979). ACR phantom based upon a random phantom "Wisconsin mammogrpahy phantoms". In W. Logan & E. P. Muntz (Eds.), *Reduced dose mammography*. New York: Masson.
23. DeWerd, L. A., Micka, J. A., Laird, R. W., Pearson, D. W., O'Brien, M., & Lamperti, P. (2002). The effect of spectra on calibration and measurement with mammographic ionization chambers. *Medical Physics, 29*, 2649–2654.
24. Dougherty, G. (1998). Computerized evaluation of mammographic image quality using phantom images. *Computerized Medical Imaging and Graphics, 22*, 365–373.
25. EC (1996). *European guidelines on quality criteria for diagnostic radiographic images. EUR 16260*. Luxembourg: European Commission.
26. EC (2006). *European Guidelines for Quality Assurance in Mammography Screening. Report EUR 14821*. Luxembourg: European Commission.
27. Egan, R. L., & Fenn, J. O. (1968). Phantoms for evaluating mammography techniques and roentgenographic detail. *American Journal of Roentgenology, 102*, 936–939.
28. Faulkner, K., & Law, J. (1994). A comparison of mammographic phantoms. *Brit J Radiol, 67*, 174–180.
29. Fitzgerald, M., White, D. R., White, E., & Young, J. (1981). Mammographic practice and dosimetry in Britain. *British Journal of Radiology, 54*, 212–220.

30. Freed, M., Badal, A., Jennings, R. J., de las Heras, H., Myers, K. J., & Badano, A. (2011). X-ray properties of an anthropomorphic breast phantom for MRI and x-ray imaging. *Phys Med Biol*, *56*, 3513–3533.
31. Geise, R. A., & Palchevsky, A. (1996). Composition of mammographic phantom materials. *Radiology, 198*, 347–350.
32. Gennaro, G., Ferro, F., Contento, G., Fornasin, F., & di Maggio, C. (2007). Automated analysis of phantom images for the evaluation of long-term reproducibility in digital mammography. *Physics in Medicine and Biology, 52*, 1387–1407.
33. Hammerstein, G. R., Miller, D. W., White, D. R., Masterson, M. E., Woodard, H. Q., & Laughlin, J. S. (1979). Absorbed radiation-dose in mammography. *Radiology, 130*, 485–491.
34. Hendrick, R. E. (1992). Quality assurance in mammography—accreditation, legislation, and compliance with quality assurance standards. *Radiologic Clinics of North America, 30*, 243–255.
35. Hessler, C., Depeursinge, C., Grecescu, M., Pochon, Y., Raimondi, S., & Valley, J. F. (1985). Objective assessment of mammography systems: 1. Method. *Radiology, 156*, 215–219.
36. Huda, W., Qu, G. Y., Jing, Z. X., Steinbach, B. G., & Honeyman, J. C. (2000). How does observer training affect imaging performance in digital mammography? In E. A. Krupinski (Ed.), *Medical imaging 2000*: *Image perception and performance* (Vol. 1, pp. 259–266).
37. Huda, W., Sajewicz, A. M., Ogden, K. M., Scalzetti, E. M., & Dance, D. R. (2002). How good is the ACR accreditation phantom for assessing image quality in digital mammography? *Academic Radiology, 9*, 764–772.
38. IAEA (2007). Dosimetry in diagnostic radiology: An international code of practice, technical reports series No. 457. *International Atomic Energy Agency*. Vienna, Austria, International Atomic Energy Agency.
39. IAEA (2011). *Quality assurance programme for digital mammography. IAEA human health series No 17*. Vienna: International Atomic Energy Agency.
40. ICRU. (1989). *Tissue substitutes in radiation dosimetry and measurement*. Bethesda: International Commission on Radiation Units and Measurements.
41. Kimme-Smith, C., Bassett, L. W., & Gold, R. H. (1989). A review of mammography test objects for the calibration of resolution, contrast, and exposure. *Medical Physics, 16*, 758–765.
42. Kosanetzky, J., Knoerr, B., Harding, G., & Neitzel, U. (1987). X-ray diffraction measurements of some plastic materials and body tissues. *Medical Physics, 14*, 526–532.
43. Kotre, C. J., & Porter, D. J. T. (2005). A printed image quality test phantom for mammography. *British Journal of Radiology, 78*, 746–748.
44. Law, J. (1991). A new phantom for mammography. *British Journal of Radiology, 64*, 116–120.
45. Law, J., Faulkner, K., & Smith, S. (1989). Variation of image quality with x-ray tube potential in mammography. *British Journal of Radiology, 62*, 192–192.
46. Liu, X., Lai, C.-J., Whitman, G. J., Geiser, W. R., Shen, Y., Yi, Y., et al. (2011). Effects of exposure equalization on image signal-to-noise ratios in digital mammography: A simulation study with an anthropomorphic breast phantom. *Medical Physics, 38*, 6489–6501.
47. McLean, D., Eckert, M., Heard, R., & Chan, W. (1997). Review of the first 50 cases completed by the RACR mammography QA programme: Phantom image quality, processor control and dose considerations. *Australasian Radiology, 41*, 387–391.
48. McLelland, R., Hendrick, R. E., Zinninger, M. D., & Wilcox, P. A. (1991). The American-college of radiology mammography accreditation program. *American Journal of Roentgenology, 157*, 473–479.
49. NCRP (2004). *A Guide to Mammography and Other Breast Imaging Procedures, NCRP Report 149*. Bethesda: National Council on Radiation Protection and Measurements.
50. Ng, K. H., DeWerd, L. A., & Schmidt, R. C. (2000). Mammographic image quality and exposure in South East Asia. *Australasian Physical and Engineering Sciences, 23*, 135–137.

51. Ng, K. H., Aus, R. J., DeWerd, L. A., & Vetter, J. R. (1997). Entrance skin exposure and mean glandular dose: Effect of scatter and field gradient at mammography. *Radiology, 205*, 395–398.
52. Obenauer, S., Hermann, K. P., & Grabbe, E. (2003). Dose reduction in full-field digital mammography: An anthropomorphic breast phantom study. *British Journal of Radiology, 76*, 478–482.
53. Oliveira, M., Nogueira, M. S., Guedes, E., Andrade, M. C., Peixoto, J. E., Joana, G. S., et al. (2007). Average glandular dose and phantom image quality in mammography. *Nuclear Instruments and Methods in Physical Research Section A, 580*, 574–577.
54. Pachoud, M., Lepori, D., Valley, J. F., & Verdun, F. R. (2004). A new test phantom with different breast tissue compositions for image quality assessment in conventional and digital mammography. *Physics in Medicine and Biology, 49*, 5267–5281.
55. Park, S., Liu, H., Jennings, R., Leimbach, R., Kyprianou, I., Badanoa, A., et al. (2009). A task-based evaluation method for x-ray breast imaging systems using variable-background phantoms. *Proceedings of SPIE, 7258*, L1–L9.
56. Poletti, M. E., Gonçalves, O. D., & Mazzaro, I. (2002). X-ray scattering from human breast tissues and breast-equivalent materials. *Physics in Medicine and Biology, 47*, 47–63.
57. Prionas, N. D., Burkett, G. W., McKenney, S. E., Chen, L., Stern, R. L., & Boone, J. M. (2012). Development of a patient-specific two-compartment anthropomorphic breast phantom. *Physics in Medicine and Biology, 57*, 4293–4307.
58. Ranger, N. T., Lo, J. Y., & Samei, E. (2010). A technique optimization protocol and the potential for dose reduction in digital mammography. *Medical Physics, 37*, 962–969.
59. Robson, K. J., Kotre, C. J., & Faulkner, K. (1995). The use of a contrast-detail test object in the optimization of optical-density in mammography. *British Journal of Radiology, 68*, 277–282.
60. Sharma, R., Sharma, S. D., & Mayya, Y. S. (2012). A survey on performance status of mammography machines: Image quality and dosimetry studies using a standard mammography imaging phantom. *Radiation Protection Dosimetry, 150*, 325–333.
61. Sharma, R., Sharma, S. D., Mayya, Y. S., & Chourasiya, G. (2012). Mammography dosimetry using an in-house developed polymethyl methacrylate phantom. *Radiation Protection Dosimetry, 151*, 379–385.
62. Song, S. E., Seo, B. K., Yie, A., Ku, B. K., Kim, H.-Y., Cho, K. R., et al. (2012). Which phantom is better for assessing the image quality in full-field digital mammography? American college of radiology accreditation phantom versus digital mammography accreditation phantom. *Korean Journal of Radiology, 13*, 776–783.
63. Suryanarayanan, S., Karellas, A., Vedantham, S., Sechopoulos, I., & D'Orsi, C. J. (2007). Detection of simulated microcalcifications in a phantom with digital mammography: Effect of pixel size. *Radiology, 244*, 130–137.
64. Taibi, A., Fabbri, S., Baldelli, P., di Maggio, C., Gennaro, G., Marziani, M., et al. (2003). Dual-energy imaging in full-field digital mammography: A phantom study. *Physics in Medicine and Biology, 48*, 1945–1956.
65. Theodorakou, C., Horrocks, J. A., Marshall, N. W., & Speller, R. D. (2004). A novel method for producing x-ray test objects and phantoms. *Physics in Medicine and Biology, 49*, 1423–1438.
66. Thompson, S. R., & Faulkner, K. (1991). A phantom for the measurement of contrast detail performance in film-screen mammography. *British Journal of Radiology, 64*, 1049–1055.
67. Tomal, A., Cunha, D. M., & Poletti, M. E. (2013). Optimal x-ray spectra selection in digital mammography: A semi-analytical study. *IEEE Transactions on Nuclear Science*, *60*, 728–734.
68. White, D. R. (1977). Formulation of tissue substitute materials using basic interaction data. *Physics in Medicine and Biology, 22*, 889–899.
69. White, D. R., & Tucker, A. K. (1980). A test object for assessing image quality in mammography. *British Journal of Radiology, 53*, 331–335.

70. Woodard, H. Q., & White, D. R. (1986). The composition of body-tissues. *British Journal of Radiology, 59*, 1209–1219.
71. Wu, X., Barnes, G. T., & Tucker, D. M. (1991). Spectral dependence of glandular tissue dose in screen-film mammography. *Radiology, 176*, 143–148.
72. Yaffe, M. J., Boone, J. M., Packard, N., Alonzo-Proulx, O., Huang, S.-Y., Peressotti, C. L., et al. (2009). The myth of the 50-50 breast. *Medical Physics, 36*, 5437–5443.
73. Yaffe, M. J., Byng, J. W., Caldwell, C. B., & Bennett, N. R. (1993). Anthropomorphic radiological phantoms for mammography. *Medical Progress Through Technology, 19*, 23–30.
74. Young, K. C., & Ramsdale, M. L. (1993). Evaluation of mammography image quality phantoms. *Radiation Protection Dosimetry, 49*, 171–173.
75. Young, K. C., Ramsdale, M. L., Bignell, F. (1998). Review of dosimetric methods for mammography in the UK breast screening programme. *Radiation Protection Dosimetry*, *80*, 183–186.